Research Square

Preprints are preliminary reports that have not undergone peer review.
They should not be considered conclusive, used to inform clinical practice,
or referenced by the media as validated information.

RalB degradation by dihydroartemisinin induces autophagy and IFI16/caspase-1 inflammasome depression in the human Laryngeal squamous cell carcinoma

xinli shi (sxlsunshine@sina.com)
Hebei University of Chinese Medicine
Shenghao Li
Hebei University of Chinese Medicine
Li Wang
Southwest Medicine University
Hui Li
Bethune International Peace Hospital
Zhen Li
Bethune International Peace Hospital
Weiyi Wang
Children's Hospital of Hebei Province
Jing Bai
Bethune International Peace Hospital
Yajing Sun
Bethune International Peace Hospital
Jianchun Li
Southwest Medical University
Xiaoming Li
Bethune International Peace Hospital

Research

Keywords: Dihydroartemisinin, IFI16 inflammasome, autophagy, laryngeal squamous cell carcinoma, RalB

Posted Date: April 8th, 2020

DOI: https://doi.org/10.21203/rs.3.rs-21425/v1

License: This work is licensed under a Creative Commons Attribution 4.0 International License. Read Full License

Version of Record: A version of this preprint was published on June 19th, 2020. See the published version at https://doi.org/10.1186/s13020-020-00340-y.

Abstract

Background

Interferon-inducible 16 (IFI16) /caspase-1 inflammasome activates and secretes IL-1β. However, whether the IFI16 inflammasome involved in human Laryngeal squamous cell carcinoma is still unclear. Autophagy directly removed inflammasome components and limited early IL-1β production. RalB is required for the crosstalk between inflammasome and autophagy in macrophages. Dihydroartemisinin (DHA), the main derived ingredient of artemisinin, has a variety of biological activities. The mechanism of DHA in regulation the crosstalk between IFI16 inflammasome and autophagy by inhibiting RalB expression was analyzed in order to provide clues for new therapeutic methods in laryngeal cancer.

Methods

The expression of IFI16 was analyzed by Oncomine and GEPIA databases and detected by Western blot and immunohistochemistry. The relationship between IFI16 inflammasome and autophagy was investigated by transmission electron microscopy, immunofluorescence assay, etc. in Hep-2, Cal-27 and HeLa cells with DHA treatment. Hep-2 cell xenograft tumor in nude mice were used to assess the effect of DHA on laryngeal cancer.

Results

The study was firstly reported that IFI16 was overexpressed and positively correlated with caspase-1 in laryngeal carcinoma tissues. DHA alone or in combination with cisplatin significantly inhibited inflammasome activation and reduced IL-1β production in the xenograft tumor microenvironment of Hep-2 cell xenograft tumor in nude mice. Mechanistically, we found that DHA degraded RalB by inhibiting USP33 expression, leading to triggered autophagy. Meanwhile, enhanced autophagy can reduce the expression of RalB and USP33. Therefore, DHA depresses RalB, resulting in formation a positive feedback loop between USP33 and autophagy. Further, DHA promotes autophagy, which suppresses the IFI16/caspase-1 inflammasome activation and IL-1β production.

Conclusions

Therefore, our findings demonstrate that DHA may act as a RalB inhibitor to regulate the crosstalk between autophagy and IFI16/caspase-1 inflammasome, which inhibits IL-1β production in tumor microenvironment.

1. Background

Laryngeal squamous cell carcinoma (LSCC) is a common malignant tumor of head and neck squamous cell carcinoma (HNSCC), accounting for about 5.7–7.6% of all HNSCC [1]. The incidence rate has gradually increased in recent years. At present, although surgery remains the main treatment modality for LSCC, chemoradiation is often needed in advanced and recurrent and/or metastatic cases. However, dose-dependent drug toxicity and tolerance restrict the effect of chemotherapy on laryngeal cancer. Therefore, it is necessary

to further explore the molecular mechanism of tumor progression and therapeutic resistance of LSCC, along with the associated new therapeutic strategies.

Long-term inflammatory microenvironment can promote tumor growth. IL-1β is an important molecule involved in the inflammation, carcinogenesis and tumor progression. Some hazardous signals act as the triggers to activate the sensor proteins leading to the formation of inflammasome in the cytoplasm. Inflammasome provides the scaffold to recruit pro-caspase-1, which is cleaved to activate caspase-1, leading to pyroptosis and the production of IL-1β and Il-18 [2]. The pyrin and HIN domain-containing (PYHIN) protein family (for example, absent in melanoma [AIM2], and interferon-inducible 16 [IFI16]) is one of the sensors for inflammasome activation [3]. Recently, it has been found that lower AIM2 expression was negatively correlated with higher p-STAT3 expression in the human hypopharyngeal squamous cell carcinoma (HSCC) tissue samples from 111 patients with HSCC, and combined analysis revealed that the patients with low AIM2 and high p-STAT3 levels had the worst survival rate [4]. IFI16, as a member of PYHIN family, can recognize double strand DNA (dsDNA) from various sources, assemble inflammasome, activate pro-caspase1, release IL-1β, and induce pyroptosis [5]. However, whether the IFI16 inflammasome is involved in LSCC progression and DHA treatment is still unclear.

Autophagy directly removed inflammasome agonists and components, limited early IL-1β production, and inhibited the activation of inflammasome [6]. For example, knockout *ATG16L1* reduced the secretion of IL-1β in mice [7]. RalB is activated when combined with GTP, thus it can promote the formation of autophagosome [8]. Ras-gene mutation is common in human laryngeal carcinoma. Ras activated three downstream effectors: RAF-MEK-ERK, PI3K-AKT-mTOR and the Ras-like (Ral). Ral is a small GTPase in Ras superfamily. There are two Ral genes of *RALA* and *RALB* in human cells. Elevated expression and activation of Ral was observed in various types of human cancers, regardless of their *RAS* mutation statuses [9]. Targeting of Ras-Ral signaling axis is a potential therapeutic strategy for Ras-driven human cancers. RalB, the key of the Ras-Ral axis, is required for the crosstalk between AIM2 or NLRP3 inflammasomes and autophagy in macrophages [10]. The blockage of RalB would make more important contribution than RAF and PI3K pathways [11]. Therefore, RalB inhibitors represent developing novel agents for cancer therapy [12]. PI3K and RAF inhibitors have already been seen in human cell lines and mouse models [13]. However, the therapies targeting Ras-RalB signaling axis are not available yet.

As FDA-approved antimalarial drug, dihydroartemisinin (DHA) is the main derived ingredient of artemisinin, a natural product from the Chinese herb of *Artemisia annua* L. [14]. DHA is a metabolite produced in the liver from artesunate and artemether, two other artemisinin derivatives [15]. DHA has a variety of biological activities such as anti-inflammation [16], anti-tumor [17] and so on. DHA strongly inhibited viral-induced tumor formation in the oral mucosa of the dogs treated with the canine oral papillomavirus [18]. Our previous studies have confirmed that DHA lead to autophagy and the death of human tongue squamous cell carcinoma (TSCC) cells *in vitro* and *in vivo* [19]. Recently, our group showed that DHA induces activation of AIM2 inflammasome in HepG2215 cells of human hepatocellular carcinoma and autophagy in HeLa cells[20, 21]. DHA has selective toxicity to tumor cells and is likely to become an anticancer drug with low toxicity, high efficiency and low cost [22, 23]. According to the results of previous work, the mechanism of DHA in regulation the crosstalk between IFI16 inflammasome and autophagy by inhibiting RalB expression was analyzed in order to provide clues for new therapeutic methods in laryngeal cancer.

2. Materials And Methods

2.1 Cell line and treatment

Human laryngeal carcinoma Hep-2 cells, tongue squamous cell carcinoma Cal-27 cells, cervical cancer HeLa cells were purchased from American Type Culture Collection (Manassas, VA, USA) and cultured in DMEM (Gibco/Thermo Fisher Scientific, Beijing, China) supplemented with 10% fetal bovine serum (Gibco/Thermo Fisher Scientific), 100 U/ml penicillin and 100 μg/ml streptomycin at 37 ℃ and 5% CO_2 in an atmosphere of 100% humidity.

DHA (TCI, Japan), etoposide (Sigma-Aldrich, St Louis MO, USA), 3-MA (Sigma-Aldrich), and rapamycin (Sigma-Aldrich) were dissolved in DMSO (Sigma-Aldrich) and stored at -20°C.

2.2 Bioinformatics Prediction

The Oncomine database (www.oncomine.com) was used to predict the DNA levels of inflammasome sensors in HNSCC and normal tissues. Then, Gene Expression Profiling Interactive Analysis (GEPIA) (http://gepia.cancer-pku.cn/) was employed to forecast the potential correlation between mRNA expression levels in HNSCC.

2.3 Cell Viability Assay

Hep-2 cells were seeded in 96-well plates (1×10^4 cells/well) and treated with DHA at different concentrations (5, 10, 20 and 40 μM) for 12, 24, 36, and 48 h. Cell viability was determined with Cell Counting Kit-8 (CCK-8, Dojindo Molecular Technology, Japan) according to the manufacturer's protocol. Finally, optical density (OD) was monitored by a Multiskan Spectrum Microplate Reader (Thermo Fisher Scientific, Inc.) at 450 nm, with 650 nm as the reference wavelength. The cell viability values were calculated as previously described [24]. IC_{50} values were obtained from the cytotoxicity curves using the SOFTmax PRO software.

2.4 Colony Formation Assay

Hep-2 cells were treated with or without 20.2 μM DHA for 24 h. After treatment, cells were trypsinized and replated into 60 mm dishes at 600 cells per dish. After they were cultured for 14 days, the cell colonies were fixed with chilled methanol, colored by Giemsa staining, and counted under the anatomical microscope. Cloning with a diameter not less than 60 μm is considered a clone.

2.5 Transmission Electron Microscopy

Hep-2 cells were treated with 20.2 μM DHA for 24 h, then the treated cells were collected, and fixed with 3% glutaraldehyde, postfixed with 1% OsO_4 (Sangon Biotech), dehydrated in acetone, and embedded in Epon 812

(Nissin EM, Tokyo). Ultrathin sections were stained with 2.0% uranyl acetate/lead citrate, and observed under transmission electron microscope (Hitachi, Ltd., Tokyo).

2.6 Immunofluorescence Assay

Hep-2 cells were cultured for 24 h on glass coverslips in 24-well plates (2×10^5 cells/well) with or without treatment with DHA. The samples were fixed, perforated, blocked, and incubated with primary antibody at 37 ℃ for 1 h and then with corresponding secondary antibody at 37 ℃ for 1 h. The primary antibody used in this study included rabbit anti-LC3B antibody (#2775, CST, diluted at 1:400). The used secondary antibodies were Alexa Fluor1 488-conjugated donkey anti-rabbit IgG antibody (Invitrogen Life Technologies, 1:400). Cytoskeleton was stained with phalloidine (Sigma, St Louis, MO, USA) and incubated at 37℃ for 1 h. Cells were counterstained with 4', 6-diamidino-2-phenylindole dihydrochloride (DAPI) (10 μg/ml) (Sigma, USA). Images were captured via a fluorescence microscope (Olympus BX51, Japan), and assessed by confocal microscopy.

2.7 Western Blot Analysis

These cells were seeded in 6-well plates (3×10^5 cells/well), treated as described above. Whole-cell extracts were directly lysed in SDS sample buffer (50 mM Tris-HCl pH 6.8, 1% SDS, 10% glycerol, 5% β-mercaptoethanol, 0.01% bromophenol blue). Total protein was isolated using RIPA lysis buffer (Solarbio, China) from xenografts in mice, 3 fresh biopsy specimens of laryngeal carcinoma tissues and adjacent normal laryngeal tissues. Protein concentrations were determined by the BCA method. The primary antibodies were mouse anti-IFI16 monoclonal antibody (ab50004, Abcam, diluted at 1:1000), rabbit anti-Caspase-1 antibody(#2225, CST, diluted at 1:500), rabbit anti-IL-1β monoclonal antibody (ab2105, Abcam, diluted at 1:1000), rabbit anti-LC3B antibody (#2775, CST, diluted at 1:400), rabbit anti-Beclin-1 antibody (#3495, CST, diluted at 1:400), rabbit anti-USP33 antibody (ab71716, Abcam, diluted at 1:2000), rabbit anti-RalB antibody (ab129077, Abcam, diluted at 1:1000), rabbit anti-GAPDH polyclonal antibody (#2118, CST, diluted at 1:1000), and rabbit anti-β-actin antibody (BE0021, Bioeasy, diluted at 1:5000). The secondary antibody was goat anti-rabbit IgG-HRP (ZB-2301, ZSGB-BIO, diluted at 1:5000) and goat anti-mouce IgG-HRP (ZB-2305, ZSGB-BIO, diluted at 1:5000). The bands were detected by ECL (enhanced chemiluminescence) detection systems (Vilber, Fusion FX5 Spectra, France). The band intensity was measured by the Image-Pro Plus v6.0 software (Media Cybemetic, USA).

2.8 Patients And Tissue Specimens

Paraffin-embedded tissue samples from 36 patients with LSCC were obtained from the dissected tissues in the archives of the Department of Otolaryngology-Head and Neck Surgery, Bethune International Peace Hospital (Shijiazhuang, China) between 2014 and 2015.

The inclusion criteria of the patients were as follows: i) A definite pathological diagnosis of LSCC; ii) no anticancer treatment (including chemoradiotherapy or biotreatment) before laryngectomy; iii) the absence of

common diseases such as diabetes, hypertension, coronary heart disease (CHD), and no history of long-term drug use; iv) the availability of formalin-fixed, paraffin-embedded tissues; and v) the availability of complete clinicopathological and follow-up data.

The 36 patients with HSCC were aged from 31 to 79 years with the mean age of 58 years. The clinicopathological characteristics of the HSCC patients are summarized in Table 2. The clinical stage of tumors was evaluated on the basis of the laryngeal cancer staging system of the American Joint Committee on Cancer (AJCC) in 2017. The surgical procedures for local LSCC involved the resection of tumor with or without the preservation of laryngeal function.

The study was approved by the Medical Ethics Institute of Bethune International Peace Hospital (Permit number: 2017-KY-02). All the samples were anonymous. Moreover, the fresh tissue specimens from 3 LSCC and the corresponding adjacent normal laryngeal tissues were collected for Western blotting at our institute in 2016. The corresponding adjacent normal laryngeal tissue with a 0.5 cm of cancer resection margin was selected during surgery. Postoperative pathology confirmed that this tissue was non-cancerous.

2.9 Establishment Of Xenograft Tumors And Treatment Of Animals

Female BALB/c nude mice (Vital River Laboratory Animal Technology Co. Ltd., Beijing) at the age of 5–6 weeks were used. Each mouse was subcutaneously inoculated with 1×10^7 Hep-2 cells in the left inguinal area to establish the xenograft tumor. When the average tumor size reached 5 mm in diameter, the tumor-bearing mice were randomly distributed into four different groups with six animals in each group. The mice in the DHA group received intraperitoneal injection of DHA in DMSO (25 mg/kg), once daily for five consecutive days per week for 21 d. The mice in the DDP group were injected DDP (2 mg/kg) intraperitoneally once every 2 days. DHA + DDP After 2 hours of DHA injection (25 mg/kg), DDP (2 mg/kg) was injected intraperitoneally [25]. The mice in the normal control (NC) group were intraperitoneally injected with 0.1% DMSO in physiological saline. Tumor size and body weight of each animal were measured every 5 days throughout the study. Tumor volume was calculated by the formula: V (mm^3) = $width^2$ (mm^2) × length (mm) × 0.5. The inhibition rate of tumor growth was calculated by the formula (1-the average tumor weight of the experimental group / the average tumor weight of NC group) × 100%. During the treatment, no mice died from tumor loading. After 21 days of treatment, all animals were sacrificed by cervical dislocation at the termination of experiments, and the tumors were removed, weighed, fixed in 4% paraformaldehyde, and embedded in paraffin.

All animals were maintained in SPF facility with the constant temperature (22–24℃) and a dark-light cycle of 12 h/12 h, and housed in plastic cages. The protocol was approved by the Ethics Committee for Animal Experiment of Bethune International Peace Hospital (Permit number: 2017-KY-18).

2.10 Immunohistochemistry (IHC)

For histological examination, all paraffin-embedded tissue samples were cut into 4 μm serial sections on glass slides, and baked at 70℃ for 15 min, followed by dehydration with gradient ethanol. Then, antigen retrieval was performed by heating to 121 ℃ for 3 min in 10 mmol/l citrate buffer (pH 6.0) with an autoclave. After the endogenous enzyme was inactivated by hydrogen peroxide (0.3%), the sections were incubated with normal goat serum at room temperature for 15 min, and incubated with mouse anti-IFI16 monoclonal antibody (ab50004, Abcam, diluted at 1:200), rabbit anti-Caspase-1 antibody(#2225, CST, diluted at 1:200), or rabbit anti-IL-1β monoclonal antibody (ab2105, Abcam, diluted at 1:200) overnight at 4 °C. PBS was used as the negative control for the primary antibody. The sections were rinsed with PBS for 3 times, and then incubated with the secondary antibody at 37 °C for 45 min. After they were rinsed with PBS, the sections were developed with 3, 3-diaminobenzidine (DAB) Kit (ZLI-9018, ZSGB-BIO, China) for 5–10 min, and washed with tap water. Next, the sections were counterstained with hematoxylin, desalinated by dilute hydrochloric acid, and rinsed for 5 min. Subsequently, the sections were dehydrated, cleared, mounted, and examined with a microscope. The results of immunohistochemistry were examined by 2 senior histopathologists using the double blind method. Cell cytomembrane/ cytoplasm stained with light yellow or tan were regarded as positive cells.

IHC staining was scored according to the following method: According to the staining intensity of immunohistochemistry, negative was scored as 0 point, light yellow as 1 point, moderate yellow as 2 points, and tan as 3 points. The percentage of positive cells in total cells of ≤ 5% was scored as 0, that of 6%-25% was scored as 1, that of 26%-50% was scored as 2, and that of > 50% was scored as 3 points. The judgment of protein expression is based on both the staining intensity and positive cell rate, and the product of these two values was calculated. After the multiplication of the two scores, they were divided into two groups: the high expression group was defined as the product was ≥ 3 points, and the low expression group was defined as the product was < 3 points.

2.11 Statistical Analysis

All statistical tests were performed by SPSS19.0 statistics software (SPSS, Chicago, IL). All *in vitro* experiments were repeated for at least three times. Data were presented as means ± SD. When more than two groups were enrolled, the mean values were compared between each two groups with one-way ANOVA or student's t test. The IFI16 and caspase-1 expressions in laryngeal carcinoma tissues and that of IL-1β protein in tumor-xenograft from mice were analyzed by Pearson's χ^2 test. Differences with $P < 0.05$ were considered statistically significant.

3. Results

3.1 Gene expression and transcription levels of inflammasome sensors in patients with HNSCC

Sensors for inflammasome activation can be classified as members of PYHIN protein family or the NOD-like receptor (NLR) protein family (For example, NLRP1, NLRP3, NLRC4, NLRC5, NLRP6, NLRP12, NOD1 and NOD2). In order to screen the expression differences of these molecules, we conducted bioinformatics

analysis. Oncomine database (http://www.oncomine.org) is the largest oncogene chip database and integrated data mining platform at present. First, the differential gene expressions of 10 sensor genes and 2 key molecules of the pathway in TCGA Head-Neck database were investigated (n = 364).

The expression of two ALRs (*IFI16 and AIM2*) and three (*NLRP3, NLRC4 and NOD1*) of eight NLR genes was significantly upregulated in 290 HNSCC when compared with 74 normal controls ($P < 0.05$, Table 1). Two ALRs (*IFI16 and AIM2*) and three NLR genes (*NLRP3, NLRC4 and NOD1*) was changed by less than 2 folds in gene expression levels (Table 1). No significant difference in the expression of the NLR genes (*NLRP1, NLRP6, NLRP12, NOD2*) was observed in TCGA Head-Neck database ($P > 0.05$, Table 1).

Table 1
Analysis of differences in expression levels of inflammasome related molecules in HNSCC by Oncomine Database

	Head-Neck carcinoma VS. Normal			**Head-Neck carcinoma VS. Buccal mucosa**			**Head-Neck carcinoma VS. Normal**		
	TCGA Head-Neck database(n = 290)			Ginos Head-Neck database (n = 54)			Cromer Head-Neck database (n = 38)		
	Fold change	P-value	t-test	Fold change	P-value	t-test	Fold change	P-value	t-test
IFI16	1.048	1.71E-11	6.889	3.115	9.22E-15	13.011	1.435	0.17	1.117
AIM2	1.048	1.71E-11	6.882	5.674	6.51E-14	11.201	2.028	0.001	3.912
NLRP1	-1.035	1	-4.674	1.674	0.037	1.878	1.089	0.428	0.192
NLRP3	1.053	3.73E-12	7.133	1.4551	0.035	1.879	1.555	0.192	0.976
NLRC4	1.033	2.02E-08	5.633						
NLRC5	1.001	0.443	0.144						
NLRP6	-1.064	1	-7.355						
NLRP12	-1.017	0.994	-2.53						
NOD1	1.08	1.64E-19	9.62	2.322	1.12E-04	5.034			
NOD2	-1.005	0.747	-0.664	-1.72	1	-3.866			
CASP1	-1.079	1	-6.227	1.445	4.26E-04	3.548	1.325	0.215	0.869
IL1B	1.028	2.40E-06	4.661	2.801	1.77E-08	6.605	4.908	0.002	5.574

Table 2
Association of IFI16 expression with the clinicopathological characteristics of patients with LSCC

Variable	All patients	IFI16 protein				*P*-value
		-	+	++	+++	
Age at surgery						$P = 0.611 > 0.05$
<60	17	0	7	3	7	
≥60	19	0	8	6	5	
Sex						$P = 0.826 > 0.05$
Male	31	0	13	8	10	
Female	5	0	2	1	2	
Histological grade						$P = 0.003 < 0.05$
I (Well)	10	0	0	3	7	
II (Moderate)	25	0	15	5	5	
III (Poor)	1	0	0	1	0	
Tumor stage						$P = 0.127 > 0.05$
T status						
T1/T2	28	0	10	7	11	
T3/T4	8	0	5	2	1	
N status						$P = 0.107 > 0.05$
N0	32	0	12	8	12	
N1/N2/N3	4	0	3	1	0	
M status						
M0	36	0	15	9	12	
M1	0	0	0	0	0	

The findings in TCGA Head-Neck database were confirmed in Ginos Head-Neck database (n = 54) with 41 HNSCC and 13 Buccal Mucosas. It was found that the mRNA expression levels of *IFI16, AIM2, NLRP3, and NOD1* were significantly upregulated in Ginos Head-Neck database (n = 54) ($P < 0.05$, Table 1). ALRs (IFI16 and AIM2) was more pronounced (> 2-fold) than NLR (*NLRP3 and NOD1*) (Table 1). Moreover, the expression levels of IFI16 (> 3-fold) and AIM2 (> 5-fold) were increased to a much greater extent than those of NLRP3 (1.4-fold) and NOD1 (2.3-fold) in HNSCC versus the control buccal mucosas (Table 1). Similarly, the mRNA

expression levels of *CASP1* and *IL1B* were significantly upregulated in Ginos Head-Neck database (n = 54) ($P < 0.05$, Table 1).

Furthermore, the transcriptional levels of 12 genes in cancers were compared with those in normal samples by using Oncomine database (Fig. 1A). It was found that IFI16 and AIM2 were significantly upregulated in patients with cancers (Fig. 1A).

The mRNA expression of 12 inflammasome molecules was compared between HNSCC and control tissues using GEPIA (Gene Expression Profiling Interactive Analysis) database (http://gepia. cancer-pku.cn/). The results indicated that the expression levels of 12 inflammasome molecules were higher in HNSCC tissues than in normal tissues. Furthermore, the expression levels of *IFI16*, *AIM2*, *NLRP1*, *NLRC5*, and *IL1B* were significantly upregulated (Fig. 1B and 1C). As the PYHIN inflammasomes showed the strongest and the most significant upregulation in patients with HNSCC, for our further investigation, we focused on the 2 most described PYHIN inflammasome sensor subtypes AIM2 and IFI16 in the tissues from patients with HNSCC and controls.

Oncomine was used to further analyze the coexpression of mRNA of inflammasome pathway molecules such as IFI16, AIM2 and IL1B in HNSCC. The results showed that the co-expression index of IFI16 (0.739) in HNSCC was higher than that of other molecules such as AIM2 (0.699) and IL-1β (0.611) in the inflammasome pathway.

3.2 Positive correlation between the expressions of IFI16 and caspase-1 in laryngeal carcinoma

Western blot was performed to test the expression of IFI16, caspase-1, and IL-1β protein in 3 pairs of primary laryngeal carcinoma and their normal para-laryngeal tissues collected from 3 patients with laryngeal cancer after surgery. The significantly increased expression of IFI16 (2.32 ± 0.12-fold), caspase-1 (1.85 ± 0.13-fold), and IL-1β protein (1.93 ± 0.10-fold) was detected in laryngeal cancer tissues compared with those in adjacent tissues (Fig. 2A and 2B). The data is consistent with the previous studies in Fig. 1. These results showed that IFI16 inflammasome is more highly expressed in laryngeal cancer than those normal tissues. Therefore, IFI16 inflammasome was selected as a predictive target on laryngeal cancer.

The production of activated caspase-1 is one of the important events in the activation of inflammasome [26]. First, the expression of IFI16 was analyzed with tumor stage for HNSCC. However, IFI16 did not significantly differ (Fig. 2C). Then, GEPIA dataset was used to analyze the correlation between IFI16 and caspase-1 in HNSCC, and it was found that the level of IFI16 was positively correlated with the level of caspase-1 ($R = 0.21$, $P < 0.01$) (Fig. 2D). The correlation between IFI16 and caspase-1 expression was further analyzed via immunohistochemistry for 36 biopsy specimens of laryngeal carcinoma tissues (Table 2). IFI16 and caspase-1 could be successfully and simultaneously expressed in those laryngeal and para-laryngeal epithelial tissues (Fig. 2E-H). Positive expression of IFI16 was primarily observed in the nucleus (Fig. 2E and 2F), and that of caspase-1 was primarily observed in the cytoplasm (Fig. 2G and 2H). The expression of IFI16 protein was detected in 36 of 36 (100%) samples (Table 2). Weak (Fig. 2E), moderate or strong staining (Fig. 2F) was detected in 6 (16.7%), 15 (41.7%), and 15 (41.7%) of the 36 samples, respectively. Correspondingly, the expression of Caspase-1 protein was detected in 33 of 36 (91.7%) samples. Weak (Fig. 2G), moderate and strong staining (Fig. 2H) was detected in 13 (36.1%), 5 (13.9%), and 15 (41.6%) of the 36 samples,

respectively. Finally, statistical analysis revealed that the level of IFI16 was positively correlated with the level of caspase-1 (rs = 0.477, $P < 0.05$) (Table 3). These results suggested that the expression of IFI16 was specifically correlated with caspapse-1-mediated pyroptosis in laryngeal carcinoma tissues.

Table 3
Correlation between expression of IFI16 and caspase-1 in the patients with laryngeal carcinoma

Capase-1	IFI16 protein			
	-	+	++	+++
-	0	0	2	1
+	0	10	5	1
++	0	2	4	2
+++	0	1	0	8
rs	0.477			
P	0.003			

3.3 DHA Inhibits Its Proliferation In Hep-2 Cells

To test the anti-proliferative effect of DHA *in vitro*, human laryngeal carcinoma Hep-2 cells were respectively exposed to DHA (5, 10, 20 and 40 μM) for 12, 24, 36 and 48 h. After this treatment, cell proliferation and cytotoxicity assay (CCK-8) was conducted to assess cell viability. It was shown that DHA with greater concentrations inhibited the growth of Hep-2 cells more significantly, and its inhibition rate also increased as time went on (Fig. 3A). The result suggested that DHA cytotoxicity was dose- and time-dependent in Hep-2 cells. However, DHA showed less inhibitory effect at 12 h compared to that at any other separate time points (Fig. 3A). Hence, 24 h treatment was the optimal overtime, with a 50% inhibiting concentration (IC50) of 20.23 μM (Fig. 3B). Next, to determine whether DHA affected long-term colony formation, a clonogenic assay was performed with 20.5 μM DHA for 24 h. Meanwhile, Hep-2 cells were treated with 40.0 μM eto poside, DNA double-strand break (DSB) agent, for 24 h and used for the positive control. It was observed that DHA-treated cell number of surviving colonies was also markedly decreased, similar to the results of Etoposide treatment (Fig. 3C). Taken together, these results suggested that DHA significantly inhibited the growth and proliferation of Hep-2 cells in dose- and time-dependent manners *in vitro*.

3.4 DHA alone or in combination significantly reduced the expression of IL-1β in serum and xenograft tumor microenvironment

The anti-tumor effect of DHA was further determined in the nude mice bearing Hep-2 tumor xenograft model. DHA (25 mg/kg/d) was administered by intraperitoneal injection for 21 days. The treatment effect was evaluated through the measurement of tumor volume. On average, DHA inhibited the tumor growth by 56.58%

(Fig. 4A). On Day 21, the mice were sacrificed and the tumor weights and volumes were measured. As expected, the weight and volume of xenograft tumor were significantly reduced in the DHA-treated mice (90.11 ± 43.42 mm^3, 121.60 ± 43.25 mg) compared with the controls (210.40 ± 86.51 mm^3, 212.92 ± 63.47 mg) (Fig. 6A). These results indicated that DHA alone noticeably inhibited the growth of Hep-2 xenograft tumor *in vivo*. Interestingly, DHA can inhibit significantly xenograft tumor in combination with cisplatin (40.28 ± 18.18 mm^3, 50.58 ± 10.98 mg) compared to the DDP-treated mice (51.81 ± 38.57 mm^3, 58.58 ± 39.31 mg), suggesting that DHA enhanced the anti-tumor effect of cisplatin (Fig. 4A). Meanwhile, the changes in body weight are not obvious in the tumor-bearing mice from the 1st to 21th days (Fig. 4B). Therefore, these results showed that DHA alone or in combination significantly inhibited the growth of xenograft tumor in nude mice.

Higher level of IL-1β in peripheral blood mononuclear cell (PBMC) cultures isolated from venous blood in the patients with laryngeal carcinoma is associated with lower 3-year and 5-year survival [27]. When the level of IL-1β measured in serum, it was detected that depressed IL-1β expression was significant in DHA-treated mice (123.30 ± 7.39 pg/ml) compared to the NC group (150.74 ± 49.63 pg/ml), and that IL-1β expression was not distinct in DDP (156.33 ± 46.18 pg/ml) or DHA in combination with DDP (146.22 ± 52.91 pg/ml) (Fig. 4C). However, DHA significantly inhibited IL-1β production when it was used in combination with DDP compared to the DDP group (Fig. 4C). In short, DHA reduced IL-1β secretion in the serum from nude mice with xenograft tumor when it was used singly or in combination.

Therefore, the effect of DHA on the inflammatory microenvironment of laryngeal cancer was investigated *in vivo*. Western blot analysis showed that cisplatin treatment increased the expression of activated caspase-1 and IL-1β, while DHA decreased it compared with the NC group (Fig. 4D). Meanwhile, DHA decreased the expression of activated caspase-1 and IL-1β in combination with cisplatin compared with cisplatin group (Fig. 4D). These results suggested that DHA alone or in combination significantly inhibited the inflammasome activation of xenograft tumor in nude mice.

Furthermore, cytotoxic and commonly prescribed chemotherapeutic drugs (for example, cisplatin, etoposide, doxorubicin) induced IL-1β secretion in primary mouse macrophages [28]. The analysis of IL-1β protein expression by immunohistochemistry in xenograft tumor showed that IL-1β protein expression was mainly localized to the cytoplasm in the xenograft Hep-2 cells (Fig. 4E). The result suggested that Hep-2 cells secreted IL-1β in the xenograft tumor microenvironment. Consistent with the above results in Fig. 4D, it was found that DDP promoted IL-1β production in the Hep-2 cells *in vivo* (Fig. 4F). Further, DHA alone or in combination significantly reduced the expression of IL-1β in xenograft tumor microenvironment (Fig. 4F).

3.5 DHA suppresses IFI16 inflammasome activation and promotes autophagy in vitro

The expression of IFI16 inflammasome in laryngeal cancer was further examined. As expected, DHA treatment reduced the expression levels of IFI16 and pro-caspase-1 in Hep-2 and cal-27 cells (Fig. 5A). These showed that DHA (20 and 40 μM) suppressed IFI16 inflammasome in the level of protein expression. In addition, DHA with high concentration (40 μM) showed strong inhibitory effect on the expression of IFI16 inflammasome. Meanwhile, DHA reduced the expression level of activated-caspase-1 in Hep-2 cells, but did

not in Cal-27 cells (Fig. 5A). Therefore, it was suggested that DHA inhibits the activation of IFI16 inflammasome in a concentration-dependent manner in laryngeal cancer Hep-2 cells.

Western blot analysis showed that DHA promoted the conversion of LC3-I to LC3-II (Fig. 5A), and that the expression of LC3-II was positively correlated with DHA concentration (20 and 40 μM). Moreover, DHA increased the expression level of Beclin-1 in a dose-dependent manner (Fig. 5A). Then, the number of autophagosomes and green fluorescent puncta under fluorescence microscopy was observed by immunofluorescent staining with LC3B antibidy. The result showed a significant increase in the number of autophagosomes in DHA-treated cells compared with the NC group (Fig. 5B). In order to further demonstrate the morphological induction of autophagy in DHA-treated cells, ultrastructural analysis was performed with transmission electron microscopy, as the test standard for autophagosomes. The formation of double- and multiple-membrane encapsulated components (autophagosomes) was noted in the cytoplasm. Consistent with the results of Fig. 5A and 5B, the number of autophagosomes was higher in the DHA-treated group than that in the control group (Fig. 5C). In a word, these results showed that DHA induced autophagy in Hep-2 cells.

3.6 Connecting The Inflammasome And Autophagy Pathways

Autophagy induction is dependent upon the inflammasome sensor, but not caspase-1 in macrophages [6]. To test whether autophagy may affect IFI16 inflammasome activity in Hep-2, Cal-27 and HeLa cells, the expression level of IFI16 was examined in which autophagy was blocked using the PI3K inhibitor 3-MA or enhanced by the mTOR inhibitor of rapamycin (Fig. 6A). Following rapamycin treatment, immunoblotting was used to detect that rapamycin induced a significant decrease of IFI16 in three cell lines (Fig. 6A and 6B). However, the modest amount of IFI16 was increased by blocking autophagy with 3-MA (Fig. 6A and 6B). These results suggested that when autophagy was activated or blocked, the amount of IFI16 was decreased or increased. Similar to rapamycin treatment, DHA reduced the expression level of IFI16 in the above three cancer cells (Fig. 6A and 6B). Altogether, these results indicated that the exposure to DHA triggered autophagy, which limited the IFI16 inflammasomes in cancer cells.

The activation of AIM2 or NLRP3 inflammasomes triggered RalB activation and autophagy in macrophages [10]. Next, the expression levels of RalB were measured in the Hep-2, Cal-27, and HeLa cells treated with 3-MA, rapamycin or DHA to investigated whether DHA could regulate the RalB expression (Fig. 6A). Consistent with the fractionation data of IFI16, the expression level of RalB compared to the control was decreased by augmenting autophagy through rapamycin treatment (Fig. 6A and 6B). However, the modest amount of RalB was increased by blocking autophagy by 3-MA (Fig. 6A and 6B). These results indicated that autophagy was negatively correlated with the expression level of RalB. In addition, DHA, like rapamycin, reduced the RalB expression (Fig. 6A and 6B).

The ubiquitin-specific processing protease 33 (USP33), as a deubiquitinating enzyme, controls the ubiquitylation of RalB GTPase at Lys 47 [8, 29]. Consistent with the data of RalB, the expression level of USP33 was decreased by DHA or rapamycin treatment, while not change with 3-MA (Fig. 6A and 6B). These results suggested that enhanced autophagy can inhibit the expression of USP33.

4. Discussion

IL-1β repression is necessary to reduce inflammation in the patients under chemotherapy. The present study showed that DHA, an anti-malarial drug, alone or in combination with DDP significantly reduced IL-1β production in the xenograft tumor microenvironment of Hep-2 cells in nude mice. Mechanistically, we found that DHA degraded RalB by inhibiting USP33 expression, leading to triggered autophagy. Meanwhile, enhanced autophagy can reduce the expression of RalB and USP33. Therefore, DHA depresses RalB, resulting in formation a positive feedback loop between USP33 and autophagy. Further, DHA promotes autophagy, which suppresses the IFI16 inflammasome activation and IL-1β production (Fig. 7).

IFI16 is a scaffold protein for protein-DNA and protein-protein interactions with transcription factors. Most studies have focused on the effects of IFI16 on the growth and migration of tumor in HNSCC tissue or cell lines. It was reported that there was a strong positive correlation between IFI16 and p-STAT3 in HPV-positive lesions in 224 head and neck precancerous and malignant lesions by immunohistochemistry and FISH analysis [30]. IFI16 is a downstream regulatory molecule of p-STAT3 [31]. Our previous research also confirmed that DHA decreased p-STAT3 (Tyr705) nuclear localization in the Cal-27 cells [19]. Recently, IFI16 was found to act as a DNA sensor in the surveillance of cytosolic double-stranded DNA (dsDNA) to trigger the innate immune response [32]. The DNA from diverse microbes and host DNA leaking out from the mitochondria or the nucleus acted as a danger signal in damaged cells [33]. Furthermore, the DNA sensor IFI16, as a pattern recognition receptor (PRR), has the ability to sense and bind Etoposide-induced damaged self-dsDNA in the nucleus in human HaCaT keratinocytes [34]. Caspase-1 production is one of the important events of inflammasome activation [26]. Z-VAD-FMK, Caspase-1 inhibitor, blocked T-cell apoptosis in HNSCC [35]. Inflammasome inhibitor has broad prospects in tumor therapy [36]. In line with this, the study was firstly reported that IFI16 was correlated with caspase-1 in laryngeal cancer. Consistent with our results, primary effusion B-cell lymphoma cells showed IFI16 mediated caspase-1 inflammasome activation [37]. Our study also found that DHA reduced the expression level of IFI16 in three human cancer cells of Hep-2, Cal-27, and HeLa. Further research found that DHA can also reduce the expression of pro-caspase-1 and inhibit the activation of caspase-1 in Hep-2 cells *in vitro* and IL-1β produced in tumor microenvironment *in vivo*. It is concluded that DHA can inhibit the expression and/or activation of IFI16 inflammasome in laryngeal cancer cells.

It is clear that chemotherapeutic drugs can promote the secretion of important pro-inflammatory cytokines such as IL-1β from monocytes and macrophages [28]. In tumor microenvironment, IL-1β contributes to epithelial-mesenchymal transition, which is related to drug tolerance in HNSCC [38]. For example, the suppression of IL-1β secretion by inhibiting inflammasome is expected to become a new treatment strategy in melanoma [39]. In addition, assembled inflammasomes can activate caspase-1 and cause IL-1β to be secreted from cancer cells [40]. In the present study, it was first found that in Hep-2 cancer cells, caspase-1 was involved in the processing and secretion of IL-1β by DDP treatment *in vivo*. DDP is a widely used chemotherapy drug for the clinical therapy of advanced and recurrent and/or metastatic laryngeal cancers. Furthermore, it was found that DDP increased the activation of caspase-1 and the production of IL-1β in Hep-2 cells in xenograft mice. Inflammasomes play different roles in various tissues and cells. The assembly of inflammasome activates caspase-1 and promotes cell death by pyroptosis in macrophages [26]. However, the animal model experiment of 4NQO-induced rat oral cancer proved that IL-1β changed tumor

microenvironment and inhibited cell proliferation in gene silenced (LV-shIL-1β) tumor cells [41]. Moreover, 5-Fluorouracil (5-FU)-based clinical chemotherapy increased the expression and activation of NLRP3 inflammasome in oral squamous cell carcinoma (OSCC) tissues, which then mediated the chemoresistance [42]. Meanwhile, high expression level of NLRP3 inflammasome suggested poor prognosis in 121 LSCC tumor tissues [43]. Because inflammasome plays duplex role in cancer development, targeting inflammasome has become a novel strategy for cancer treatment [44]. For example, the inhibition of NLRP3 inflammasome/IL-1β signaling pathway may help 5-FU-based adjuvant chemotherapy of OSCC [42]. Autophagosomes transport cytoplasmic constituents to lysosomes for degradation. Here it is shown that DHA triggered the formation of autophagosome, but inhibited the activation of IFI16 inflammasomes *in vitro*. The induction of autophagy depends on the presence of the inflammasome sensor, but not that of caspase-1 [6]. In concordance with this idea, it was found that the blockage of autophagy potentiated the activity of IFI16 inflammasome, whereas the stimulation of autophagy limited it in three human cancer cells of Hep-2, Cal-27, and HeLa.

RalB, but not RalA, is necessary and sufficient for the activation of autophagy [45]. Moreover, Ral-EGF signaling activates STAT3 through SRC tyrosine kinase [46]. Previous research by the research group found that elevated STAT3 and EGFR in the tumor tissues from HNSCC patients [47, 48]. Recently, we have found that high phosphorylated STAT3 (Tyr-705) levels had the worst survival rate in hypopharyngeal squamous cell carcinoma [4]. We have reported that DHA selectively downregulated the level of p-Jak2 and inhibited the growth of HNSCC [49] (Fig. 7). Further, DHA disrupted the nuclear translocation of p-STAT3 (Tyr-705) and promoted autophagy in Cal-27 cells [19] (Fig. 7). The activation of RalB promotes the formation of starvation-induced autophagosome in cervical cancer HeLa cells and in immortalized bronchial epithelial HBEC3-KT cells [45]. Various inflammasome stimuli triggered autophagy by activating RalB in macrophages [6]. In this study, it was shown that DHA reduced the expression level of RalB and USP33 in three different types of cancer cells. It is speculated that this effect of DHA may be a common phenomenon in tumor cells. Consistently, one group selectively designed RalB peptide inhibitors in that Ras-Ral pathway is difficult disrupted by traditional medicine [50]. The RalB-specific ubiquitin ligase, USP33 is a member of the USP deubiquitinase superfamily and controls the ubiquitylation of RalB GTPase at Lys 47, which provides a regulatory switch to trigger the autophagy or innate immune response in macrophages [8]. For example, nutrient deprivation triggers the accumulation of USP33 leading to RalB deubiquitylation, which triggers the assembly of RalB-EXO84-beclin-1 complexes that initiates autophagy. In this study, autophagy inhibited the expression of RalB and USP33 in cancer cells. DHA treatment induced a positive feedback loop between RalB /USP33 expression and autophagy.

5. Conclusion

Therefore, it is proposed that DHA may act as a RalB inhibitor and definitely anticancer strategy needs further investigations in laryngeal cancer. Furthermore, DHA regulates the crosstalk between autophagy and IFI16/caspase-1 inflammasome, which inhibits IL-1β production in tumor microenvironment.

Abbreviations

IFI16
Interferon-inducible 16

DHA
Dihydroartemisinin
LSCC
Laryngeal squamous cell carcinoma
HNSCC
Head and neck squamous cell carcinoma
PYHIN
Pyrin and HIN domain-containing
AIM2
Absent in melanoma
HSCC
Human hypopharyngeal squamous cell carcinoma
dsDNA
Double strand DNA
Ral
Ras-like
TSCC
Human tongue squamous cell carcinoma
CCK-8
Cell Counting Kit-8
NLR
NOD-like receptor
OSCC
Oral squamous cell carcinoma
5-FU
5-Fluorouracil
USP33
Ubiquitin-specific processing protease 33

Declarations

Ethics approval and consent to participate

All experimental protocols and animal handling procedures were approved by the Ethics Committee for Animal Experiment of Bethune International Peace Hospital (Permit number: 2017-KY-18). The clinical stage of tumors was approved by the Medical Ethics Institute of Bethune International Peace Hospital (Permit number: 2017-KY-02).

Consent for publication

Not applicable.

Availability of data and materials

The datasets analyzed during the current study available from the corresponding author on reasonable request.

Competing interests

The authors declare that there is no conflict of interest regarding the publication of this paper.

Funding

This work was financially supported by the Scientific Research Project of Hebei Provincial Health Planning Commission (No. 20180906), China Postdoctoral Science Fund (No.2016M603018), and the Project of Natural Fund of Hebei Province (H2017423011).

Author contribution

X.S. and X.L. designed research; S.L., L.W., H.L., J.L., X.S., Z.L., J.B., and Y.S. performed the experiments; L.W. and H.L. analyzed data; X.S. and X.L. wrote the manuscript with contributions from all authors.

Acknowledgements

Not applicable.

References

1. Bray F, et al. Global cancer statistics 2018: GLOBOCAN estimates of incidence and mortality worldwide for 36 cancers in 185 countries. CA-Cancer J Clin. 2018;68(6):394–424.
2. Veeranki S, et al. IFI16 protein mediates the anti-inflammatory actions of the type-I interferons through suppression of activation of caspase-1 by inflammasomes. Plos One. 2011;6(10):e27040.
3. Franchi L, et al. The inflammasome: a caspase-1-activation platform that regulates immune responses and disease pathogenesis. Nat Immunol. 2009;10(3):241–7.
4. Li Z, et al. Low expression of AIM2 combined with high expression of pSTAT3 is associated with poor prognosis in hypopharyngeal squamous cell carcinoma. Oncol Rep. 2019;41(4):2396–408.
5. Guo H, et al. Inflammasomes: mechanism of action, role in disease, and therapeutics. Nat Med. 2015;21(7):677–87.
6. Shi CS, et al. Activation of autophagy by inflammatory signals limits IL-1beta production by targeting ubiquitinated inflammasomes for destruction. Nat Immunol. 2012;13(3):255–63.
7. Saitoh T, et al. Loss of the autophagy protein Atg16L1 enhances endotoxin-induced IL-1beta production. Nature. 2008;456(7219):264–8.
8. Simicek M, et al. The deubiquitylase USP33 discriminates between RALB functions in autophagy and innate immune response. Nat Cell Biol. 2013;15(10):1220–30.
9. Yan C, et al. RAL GTPases: Biology and potential as therapeutic targets in cancer. Pharmacol Rev. 2018;70(1):1–11.
10. Shi C-S, et al. Activation of autophagy by inflammatory signals limits IL-1β production by targeting ubiquitinated inflammasomes for destruction. Nat Immunol. 2012;13(3):255–63.

11. Zago G, et al. RalB directly triggers invasion downstream Ras by mobilizing the Wave complex. *eLife*. 2018; 7.
12. Yan C, et al. Discovery and characterization of small molecules that target the GTPase Ral. Nature. 2014;515(7527):443–7.
13. Cox AD, et al. Drugging the undruggable RAS: Mission possible? Nat Rev Drug Discov. 2014;13(11):828–51.
14. Tu Y. The discovery of artemisinin (qinghaosu) and gifts from Chinese medicine. Nat Med. 2011;17(10):1217–20.
15. Duthaler U, et al. Evaluation of the pharmacokinetic profile of artesunate, artemether and their metabolites in sheep naturally infected with Fasciola hepatica. Vet Parasitol. 2012;186(3–4):270–80.
16. van Huijsduijnen RH, et al. Anticancer properties of distinct antimalarial drug classes. Plos One. 2013;8(12):e82962.
17. Li PC, et al. Artesunate derived from traditional Chinese medicine induces DNA damage and repair. Cancer Res. 2008;68(11):4347–51.
18. Disbrow GL, et al. Dihydroartemisinin is cytotoxic to papillomavirus-expressing epithelial cells in vitro and in vivo. Cancer Res. 2005;65(23):10854–61.
19. Shi X, et al. Dihydroartemisinin induces autophagy-dependent death in human tongue squamous cell carcinoma cells through DNA double-strand break-mediated oxidative stress. Oncotarget. 2017;8(28):45981–93.
20. Wang L, et al. Antimalarial Dihydroartemisinin triggers autophagy within HeLa cells of human cervical cancer through Bcl-2 phosphorylation at Ser70. Phytomedicine. 2019;52:147–56.
21. Shi X, et al. Dihydroartemisinin, an antimalarial drug, induces absent in melanoma 2 inflammasome activation and autophagy in human hepatocellular carcinoma HepG2215 cells. Phytother Res. 2019;33(5):1413–25.
22. Lai H, et al. Selective cancer cell cytotoxicity from exposure to dihydroartemisinin and holotransferrin. Cancer Lett. 1995;91(1):41–6.
23. Ho WE, et al. Artemisinins: Pharmacological actions beyond anti-malarial. Pharmacol Therapeut. 2014;142(1):126–39.
24. Cai X, et al. Luteolin induced G2 phase cell cycle arrest and apoptosis on non-small cell lung cancer cells. Toxicol In Vitro. 2011;25(7):1385–91.
25. Xinli Shi, et al. Antitumor effect of dihydroartemisinin on hypopharyngeal cancer in nude mice with transplanted tumor. Cancer Res Prev Treat. 2017;44(10):647–51.
26. Guo H, et al. Inflammasomes: mechanism of action, role in disease, and therapeutics. Nat Med. 2015;21(7):677–87.
27. Wong J, et al. Production of IL-1beta by bone marrow-derived macrophages in response to chemotherapeutic drugs: synergistic effects of doxorubicin and vincristine. Cancer Biol Ther. 2014;15(10):1395–403.
28. Kurebayashi Y, et al. Landscape of immune microenvironment in hepatocellular carcinoma and its additional impact on histological and molecular classification. Hepatology. 2018;68(3):1025–41.

29. Chan NC, et al. Degradation of the deubiquitinating enzyme USP33 is mediated by p97 and the ubiquitin ligase HERC2. J Biol Chem. 2014;289(28):19789–98.
30. Mazibrada J, et al. Differential expression of HER2, STAT3, SOX2, IFI16 and cell cycle markers during HPV-related head and neck carcinogenesis. New Microbiol. 2014;37(2):129–43.
31. Kim E-J, et al. IFI16 is an essential mediator of growth inhibition, but not differentiation, induced by the leukemia inhibitory factor/JAK/STAT pathway in medullary thyroid carcinoma cells. J Biol Chem. 2005;280(6):4913–20.
32. Unterholzner L, et al. IFI16 is an innate immune sensor for intracellular DNA. Nat Immunol. 2010;11(11):997–1004.
33. O'Neill LA. Sensing the Dark Side of DNA. Science. 2013;339(6121):763–4.
34. Goubau D, et al. PYHIN proteins: center stage in DNA sensing. Nat Immunol. 2010;11(11):984–6.
35. Gastman BR, et al. elucidation of intracellular apoptotic events. Blood. 2000;95(6):2015–23.
36. Zitvogel L, et al. Inflammasomes in carcinogenesis and anticancer immune responses. Nat Immunol. 2012;13(4):343–51.
37. Singh VV, et al. Kaposi's sarcoma-associated herpesvirus latency in endothelial and B cells activates gamma interferon-inducible protein 16-mediated inflammasomes. J Virol. 2013;87(8):4417–31.
38. St John MA. Inflammatory mediators drive metastasis and drug resistance in head and neck squamous cell carcinoma. Laryngoscope. 2015;125(Suppl 3):1–11.
39. Dunn JH, et al. Inflammasomes as molecular mediators of inflammation and cancer: potential role in melanoma. Cancer Lett. 2012;314(1):24–33.
40. McDonald B, et al. Intravascular danger signals guide neutrophils to sites of sterile inflammation. Science. 2010;330(6002):362–6.
41. Wu T, et al. Modulation of IL-1beta reprogrammes the tumor microenvironment to interrupt oral carcinogenesis. Sci Rep. 2016;6:20208.
42. Feng X, et al. The role of NLRP3 inflammasome in 5-fluorouracil resistance of oral squamous cell carcinoma. J Exp Clin Cancer Res. 2017;36(1):81.
43. Xue Y, et al. Correlation between the NLRP3 inflammasome and the prognosis of patients with LSCC. Front Oncol. 2019;9:588.
44. Wang Z, et al. Inflammasome and cancer. Exp Suppl. 2018;108:281–302.
45. Bodemann BO, et al. RalB and the exocyst mediate the cellular starvation response by direct activation of autophagosome assembly. Cell. 2011;144(2):253–67.
46. Goi T, et al. An EGF receptor/Ral-GTPase signaling cascade regulates c-Src activity and substrate specificity. EMBO J. 2000;19(4):623–30.
47. Wang J, et al. Expression of STAT3 and p-STAT3 in laryngeal carcinoma and its clinical significance. J Clin Otorhinolaryngol Head Neck Surg. 2007;21(3):113–5.
48. Song Q, et al. Research progress of squamous cell carcinoma of head and neck EGFR targeted therapy resistance mechanisms. J Clin Otorhinolaryngol Head Neck Surg. 2015;29(2):184–90.

49. Jia L, et al. Dihydroartemisinin as a putative STAT3 inhibitor, suppresses the growth of head and neck squamous cell carcinoma by targeting Jak2/STAT3 signaling. Plos One. 2016;11(1):e0147157.
50. Thomas JC, et al. Inhibition of Ral GTPases uusing a stapled peptide approach. J Biol Chem. 2016;291(35):18310–25.

Figures

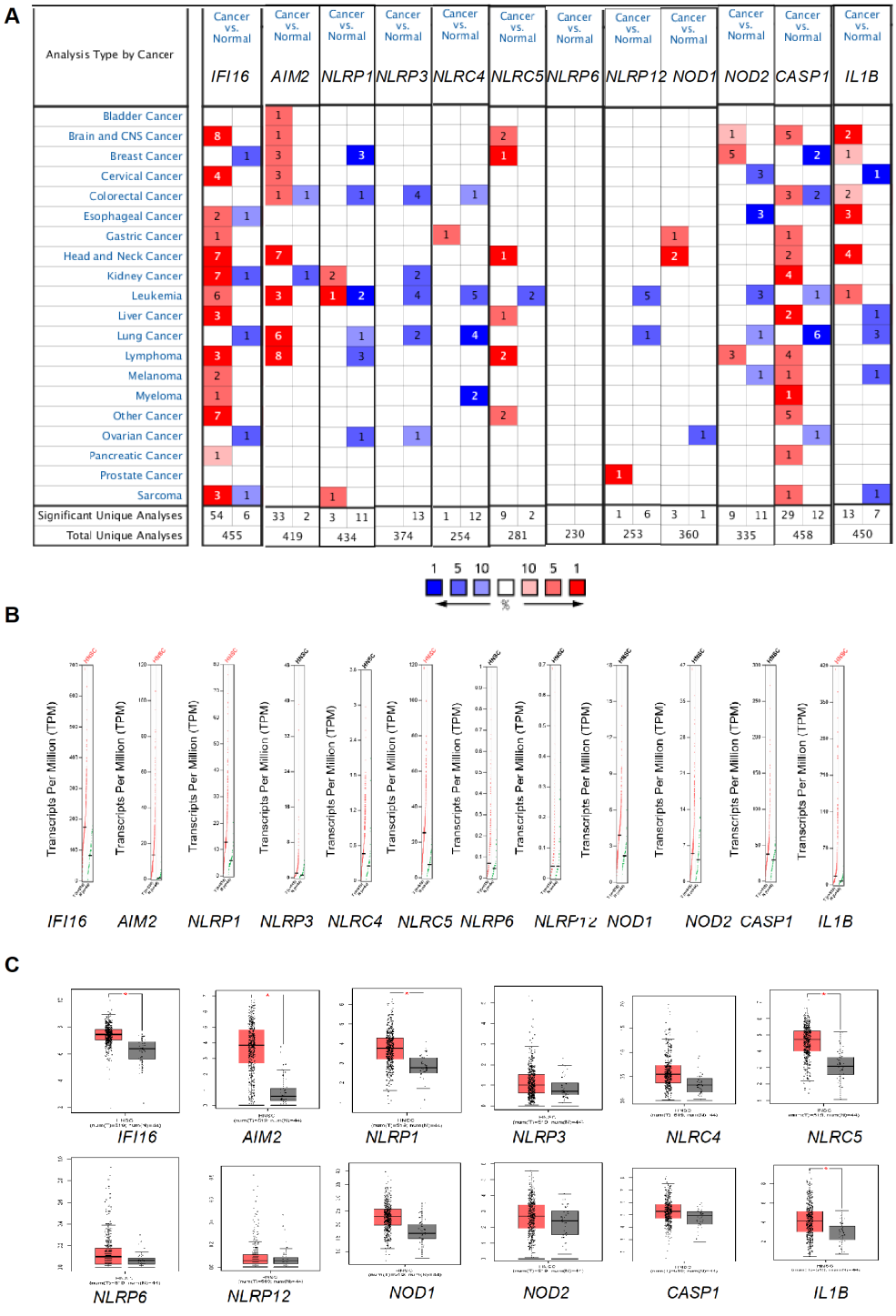

Figure 1

Gene expression and transcription levels of inflammasome sensors in patients with HNSCC. A. Oncomine analysis of the transcription levels of 12 inflammasome molecules in different types of cancers. This figure indicates the numbers of datasets with statistically significant inflammasome mRNA upregulation (red) or downregulation (blue) in different types of cancers versus the corresponding normal tissues (Threshold settings: p value, 0.05; fold change, 2; gene rank, top 10%). The numbers in the colored cells represent the numbers of dataset meeting the threshold. B and C. Different expressions of these inflammasome molecules between tumor and adjacent normal tissues from HNSCC in the GEPIA database. '*' indicates statistical significance with P<0.05. T: tumor; N: normal.

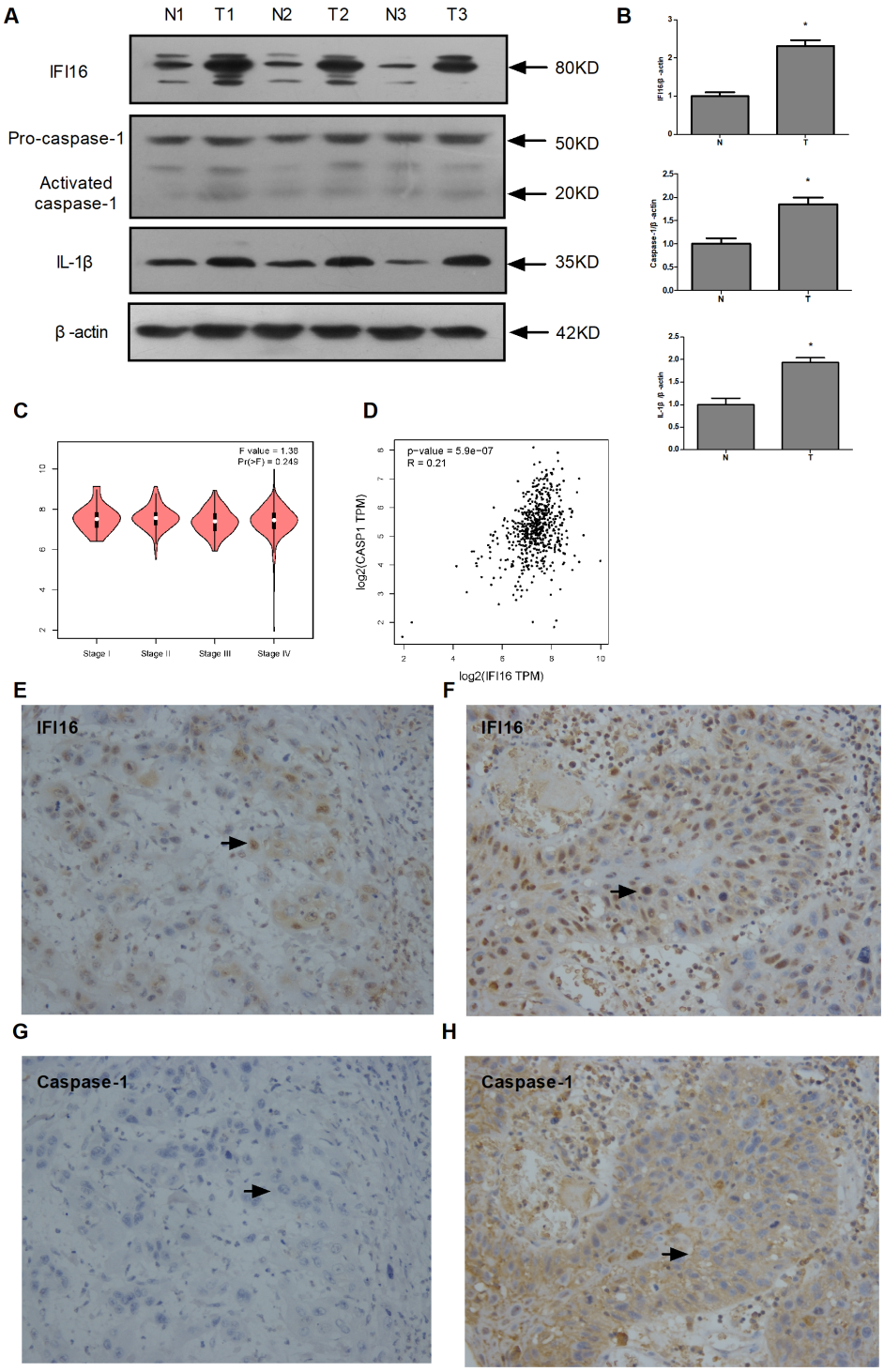

Figure 2

Positive correlation between the expression of IFI16 and caspase-1 in laryngeal carcinoma A. The protein expression of IFI16, caspase-1, IL-1β in 3 pairs of laryngeal carcinoma and adjacent normal tissues from 3 LSCC patients. β-actin served as the loading control. B. Statistical analysis of IFI16 inflammasomes. Data were shown as mean ± SD (n = 3). '*' represents that $P < 0.05$ vs. adjacent normal tissues. C. IFI16 mRNA expression in different TNM stages in HNSCC patients (GEPIA). D. The correlation between IFI16 mRNA expression and Caspase-1 in HNSCC patients in the GEPIA database. E-H. IFI16 and caspase-1 expression is analyzed via immunohistochemistry for 36 biopsy specimens of laryngeal carcinoma tissues. (E) IFI16 exhibited weak nuclear staining in 8 of the 36 (22.2%). (F) IFI16 exhibited strong nuclear cytoplasmic staining in 28 of the 36 specimens (77.8%). (G) Caspase-1 exhibited weak cytoplasmic staining in 16 of the 36 specimens (44.4%). (H) Caspase-1 exhibited weak strong cytoplasmic staining in 20 of the 36 specimens (55.6%). Original magnification, ×400. Scale bars, 25 μm, Black arrow.

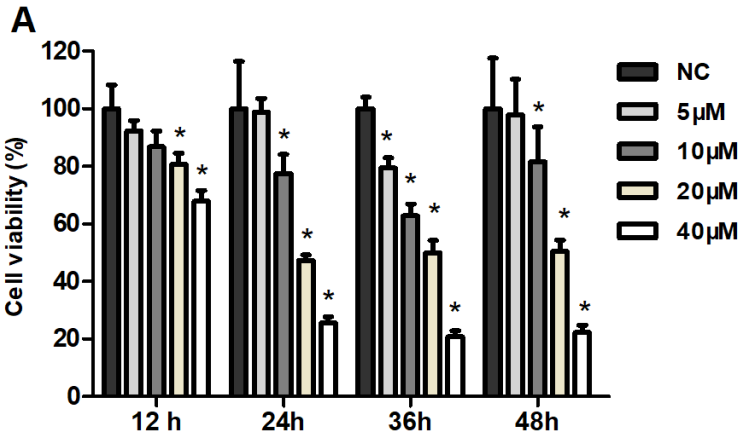

B

	IC_{50} with 95%CI	Optimum IC_{50}
24h	18.62-21.99	20.23
36h	14.81-18.10	16.37
48h	18.52-23.40	20.82

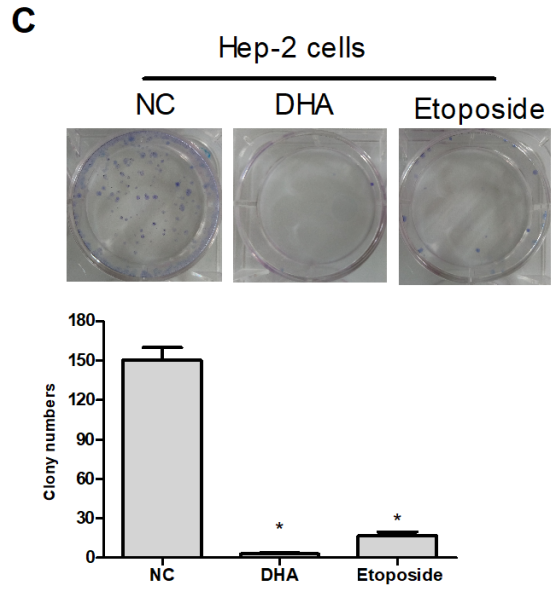

Figure 3

DHA inhibits cell proliferation in Hep-2 cells. A. CCK8 was used to test the inhibitory effect of DHA on the proliferation of Hep-2 cells. Hep-2 cells were treated with DHA as indicated (mean ± SD, n = 3). B. The IC50 values of cells were measured at 24, 36, and 48 h. IC50 values were obtained from the cytotoxicity curves using the SOFTmax PRO software. C. Representative photographs of clonogenic assay. Hep-2 cells were treated with 20.5 μM DHA, 40 μM Etoposide, and DMSO (NC group) for 24 h, respectively. All experiments were performed for at least three times. A representative result was presented. Statistical analysis of the number of

clone after 14-day incubation. The inhibition effects of growth and proliferation were calculated by number of formed cell clones. Data are shown as the mean ± SD (n = 3). *p < 0.05 versus NC group.

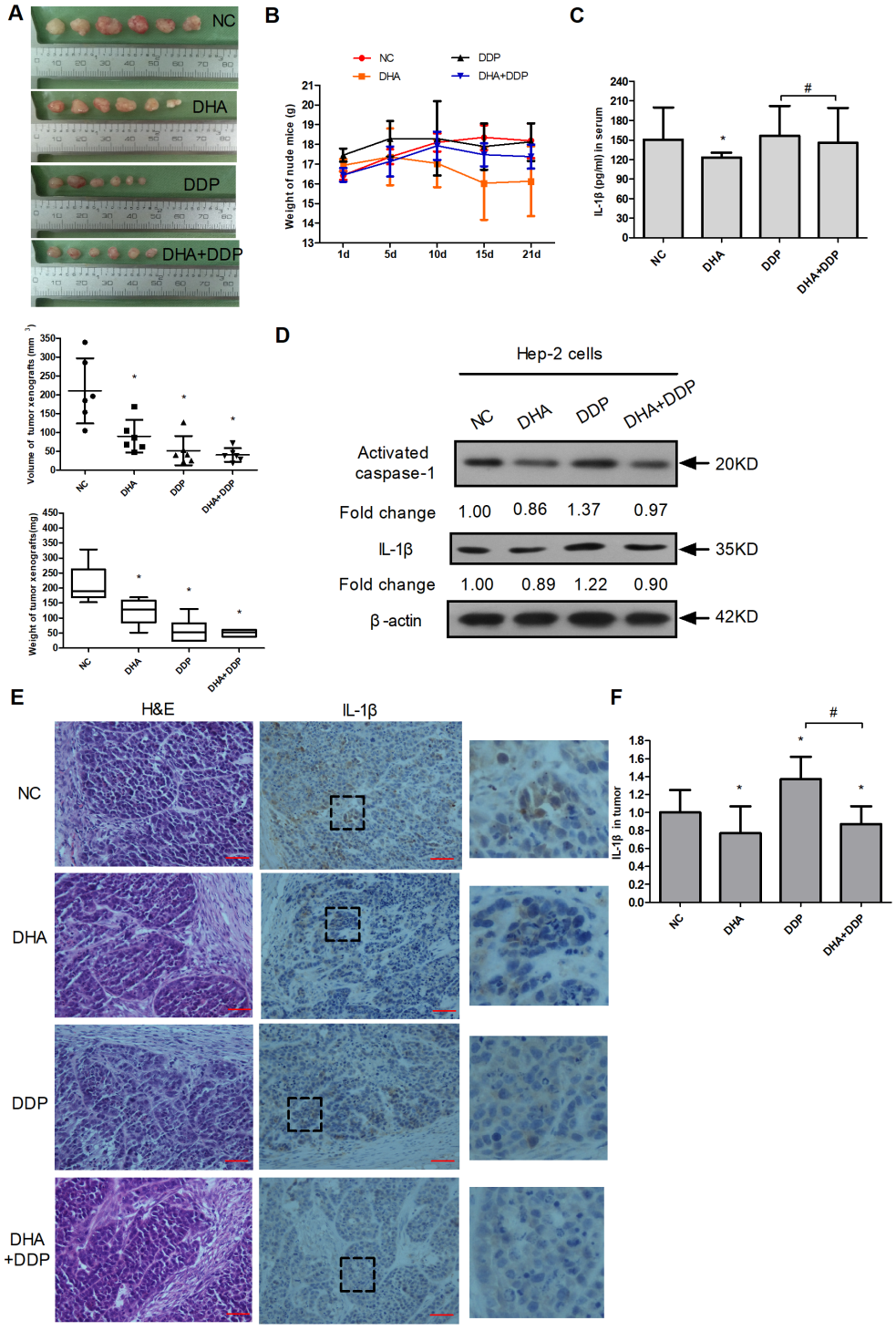

Figure 4

DHA alone or in combination significantly reduced the expression of IL-1β in serum and xenograft tumor microenvironment A. DHA noticeably inhibited the growth of Hep-2 xenograft tumor. Nude mice were inoculated with 1×107 of Hep-2 cells. When the formed tumor was palpable, the mice were randomly divided into four groups. The drug treatments were carried out according to the method section. The volume, weight

and diameter of tumor xenografts were presented when the mice were sacrificed. Tumor volume was calculated by the formula: V (mm3) = width2× length×0.5. Data were shown as means ± SD, *P < 0.05 vs. control. B. The body weight changes of tumor-bearing mice at the 1st and 21th days. C. IL-1β in the serum of nude mice was measured at the 21th day. D. Statistical analysis of caspase-1 and IL-1β expression by Western blot. Data were shown as mean ± SD (n = 3). '*' represents that P < 0.05 vs. NC group. E. Histological findings of the tumor were determined by H&E staining (left panels) and the expression of IL-1β protein was analyzed by immunohistochemistry (right panels) when the tumor-xenograft mice were sacrificed. Magnification × 400. F. Expression analysis of IL-1β protein by immunohistochemistry in nasopharyngeal carcinoma tissues.

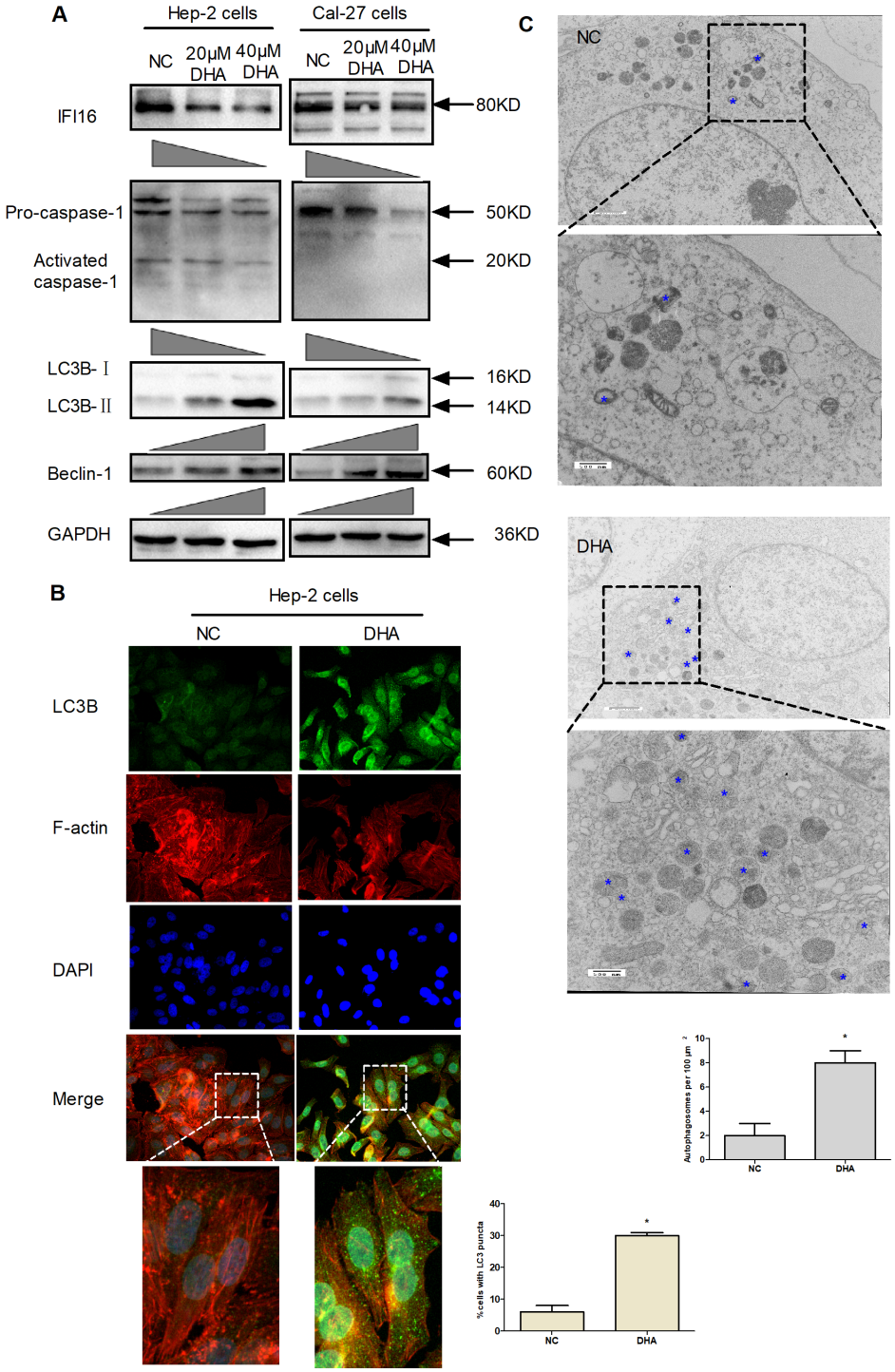

Figure 5

DHA suppresses IFI16 inflammasome activation and promotes autophagy in vitro. A. Western blot was used to detect the expression of IFI16-mediated inflammasome and LC3B in Hep-2 and Cal-27 cells. Cells that were treated as described above. GAPDH was used as the loading control. B. DHA-induced autophagosomes were detected in Hep-2 cells by immunofluorencent staining of LC3B (green) (1000×). Hep-2 Cells were treated with DHA (20.2 μM) and 0.1% DMSO (NC) respectively for 24h. F-actin (red) was stained with Phalloidine (red). Nuclei were counter-stained with DAPI (blue). The upper and bottom panels were respectively 400× and 1000×. The bar chart in the lower right corner was the statistical analysis of the autophagosomes number. A total of 200 cells were counted for each group. Data were shown as the mean±SD (n=3). * P<0.05 vs. NC group. C. Formation of autophagic vacuoles by DHA was observed under transmission electron microscope. The autophagic vacuole was indicated by blue asterisks. A total of 20 cells were counted for each group.

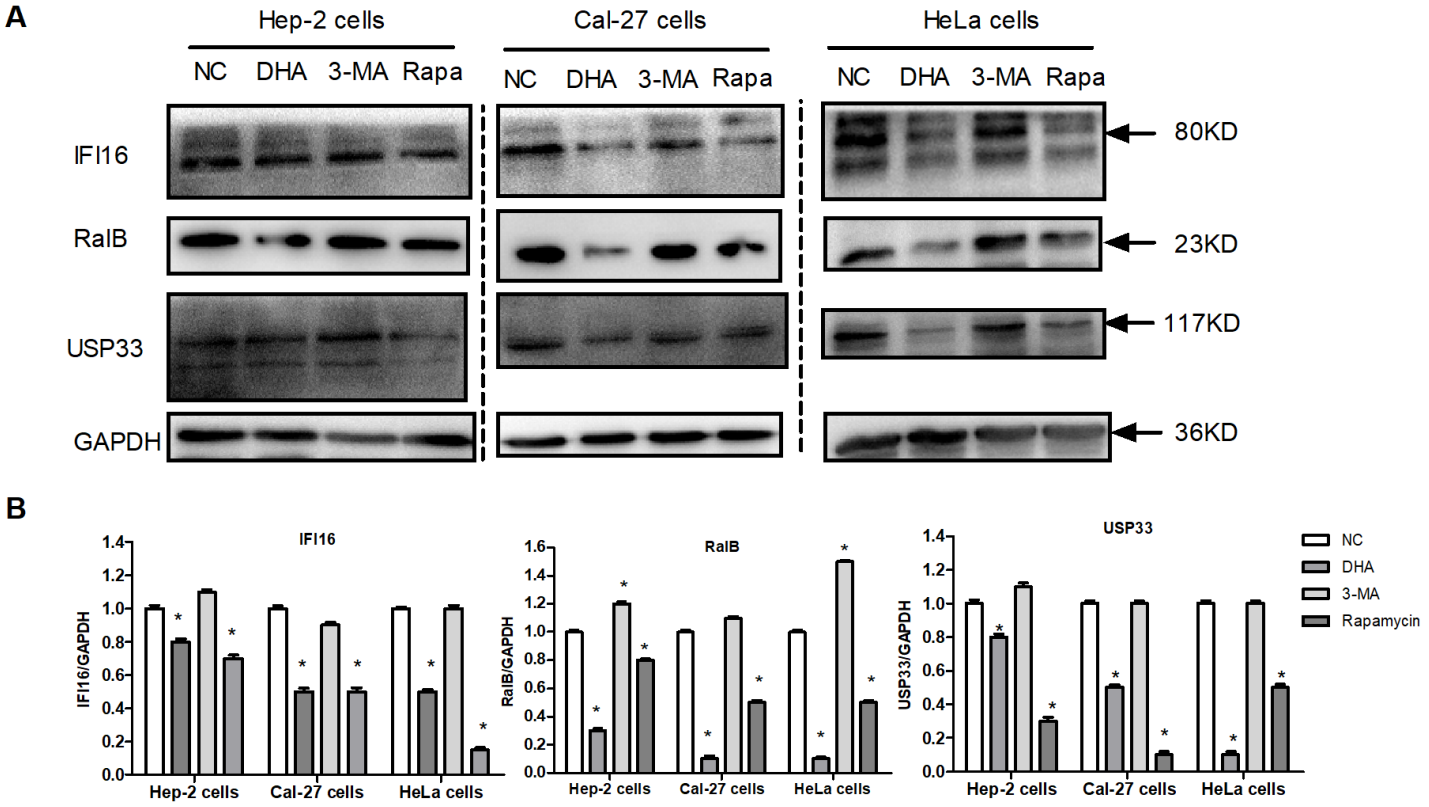

Figure 6

Connecting the inflammasome and autophagy pathways. A. Western blot was used to detect the expression of IFI16 and RalB in Hep-2, Cal-27, and HeLa cells. GAPDH was used as the loading control. Hep-2, Cal-27, and HeLa cells were treated with DHA (20.2 μM, 24.5 μM, 31 μM), and 0.1% DMSO (NC) respectively for 24h. Rapamycin (0.1 μM) acted as the autophagy activator, and 3-MA (1 mM) acted as the autophagy inhibitor. B. Statistical analysis of IFI16, RalB and USP33. Cells were treated as described above. Data were shown as mean ± SD (n = 3). '*' represents that P < 0.05 vs. NC.

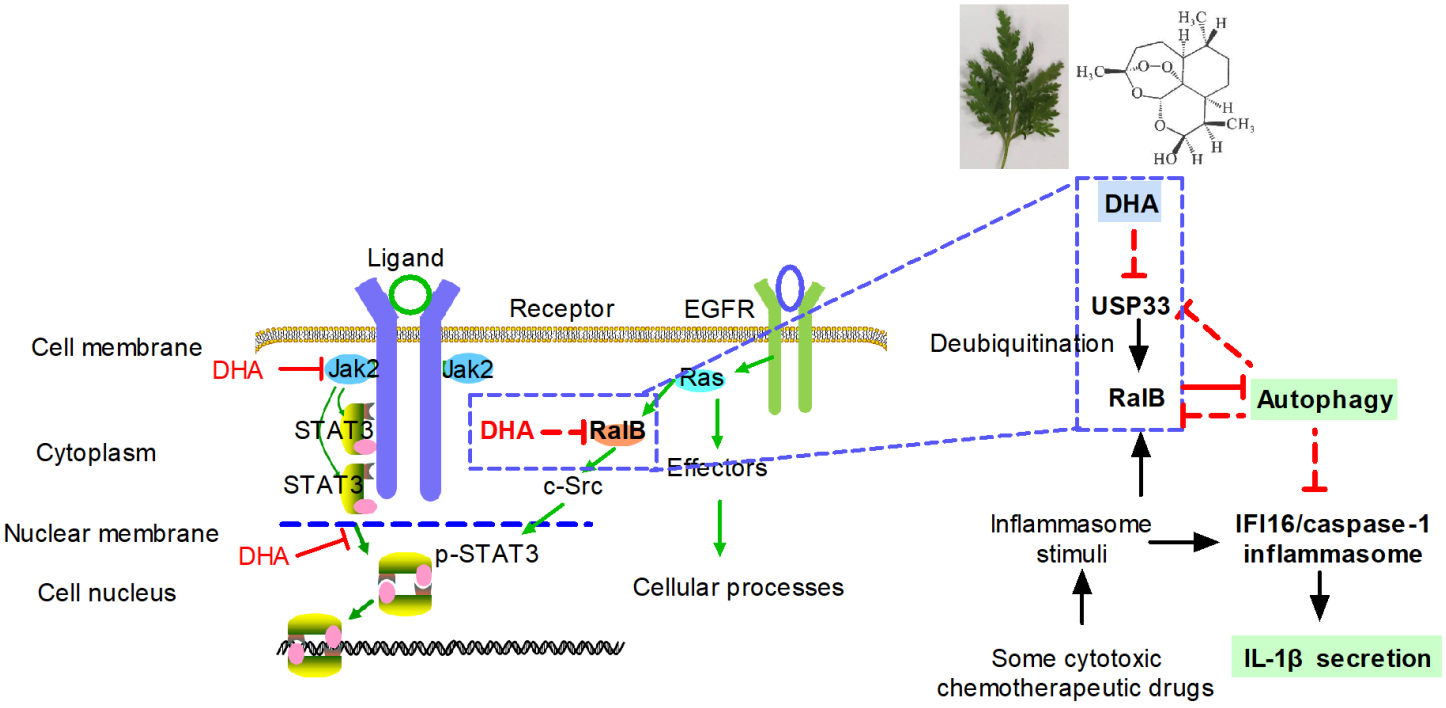

Figure 7

The mechanism model of the crosstalk between IFI16/caspase-1 inflammasome and autophagy via RalB degradation by DHA in the human laryngeal squamous cell carcinoma. Mechanically, DHA degraded RalB by inhibiting USP33 expression, leading to triggered autophagy. Meanwhile, autophagy reduced the expression of RalB and USP33. Therefore, DHA depresses RalB, resulting in formation a positive feedback loop between USP33 and autophagy. Further, DHA promotes autophagy, which suppresses the IFI16 inflammasome activation and IL-1β secretion.